IEEE Access
Multidisciplinary | Rapid Review | Open Access Journal

Received May 8, 2020, accepted May 18, 2020, date of publication May 21, 2020, date of current version June 4, 2020.

Digital Object Identifier 10.1109/ACCESS.2020.2996408

A 3D Ray Launching Time-Frequency Channel Modeling Approach for UWB Ranging Applications

TIMOTHY OTIM[1], PEIO LOPEZ-ITURRI[2,3], (Member, IEEE), LEYRE AZPILICUETA[4], (Senior Member, IEEE), ALFONSO BAHILLO[1], LUIS ENRIQUE DÍEZ[1], AND FRANCISCO FALCONE[2,3], (Senior Member, IEEE)

[1]Faculty of Engineering, University of Deusto, 48007 Bilbao, Spain
[2]Department of Electrical, Electronics, and Communication Engineering, Public University of Navarre, 31006 Pamplona, Spain
[3]Institute for Smart Cities, Public University of Navarre, 31006 Pamplona, Spain
[4]School of Engineering and Sciences, Tecnologico de Monterrey, Monterrey 64849, Mexico

Corresponding author: Timothy Otim (otim.timothy@deusto.es)

This work was supported in part by the Research Training Grants Program of the University of Deusto, and in part by the Ministerio de Ciencia, Innovación y Universidades (MCIU), Gobierno de España, Agencia Estatal de Investigación/Fondo Europeo de Desarrollo Regional, Unión Europea (AEI/FEDER, UE), under Grant RTI2018-095499-B-C31.

ABSTRACT Ultrawideband (UWB) has the ability to achieve decimetre level of ranging accuracy, hence, its wider usage nowadays in the field of positioning. In spite of the attractiveness of UWB, its performance is strongly dependent on the propagation channel. In this paper, an analysis of the the UWB channel for ranging applications using an inhouse developed 3D Ray launching (3D RL) algorithm is presented. A parametric study has been performed considering variations of cuboid size resolution of the simulation mesh, in order to analyze convergence impact on estimation accuracy, focusing on Radio frequency (RF) power levels as well as time domain characterization. The RF power results have been used to model the path-loss, small scale fading, and the power delay profile so as to obtain the statistics of the multipath channel as well as time of flight (TOF) estimation values. The results show that the 3D RL is a valuable tool to test UWB systems for ranging applications with a mean accuracy of up to 10 cm in multipath conditions considering complex scatterer distributions within the complete volume of the scenarios under test.

INDEX TERMS Ultrawideband, 3D ray launching, time of flight, ranging, channel modelling, radio frequency power levels.

I. INTRODUCTION

The Federal Communications Commission (FCC) and the International Telecommunication Union Radiocommunication sector (ITU-R) define Ultrawideband (UWB) as an antenna transmission for which the emitted signal occupies a fractional bandwidth greater than 0.2 or a bandwidth more than 500 MHz. Thanks to its several attractive properties, UWB technology has seen tremendous advances in the field of wireless communications [1], imaging [2], radar [3], networking [4], and localization [5]. For instance, the large bandwidth allows for more reliable communications by providing a high resilience to frequency selective fading. Additionally, the spectral power spreading over a high bandwidth decreases the spectral density, consequently reducing interference to existing wireless systems. Finally, thanks to concept of pulse based UWB radio, the construction of communications systems with reduced complexity in the Radio frequency (RF) architecture is now possible.

Multiple solutions have been described in order to provide localization in indoor environments, based on technologies such as Wi-Fi/WLAN, Infrared, RFID, Cameras, among others [6]. However, the use of ultra-short pulses such as in UWB enables high time resolution, providing high accuracy. Therefore, UWB positioning has the ability to achieve decimeter-level location estimates using time of flight (TOF) techniques [6]. The reason is that the high bandwidth allows accurate TOF computations and it is robust against multipaths. Consequently, a considerable part of these systems is deployed in several environments such as hospitals, residential, industrial and others [6]. This is leading to an ever increasing adoption and deployment of UWB positioning

The associate editor coordinating the review of this manuscript and approving it for publication was Prakasam Periasamy.

systems. Moreover, this necessity is likely to increase in the near future because mobile phone manufacturers such as Apple Inc are demonstrating attraction to this technology. For instance the new iPhone 11 embeds an UWB interface, and the company expects to release UWB beacons soon [7]. In spite of potential benefits of UWB, its performance is strongly dependent on the propagation channel. In fact, critical and real time applications such as positioning require line-of-sight (LOS) situations between the transmitter (Tx) and receiver (Rx) as well as a careful characterization of the channel. Therefore, to adequately deploy the necessary RF sources i.e., access points or anchors in wireless sensor networks, it is compulsory to adequately characterise the radio propagation losses as well as the time domain properties of the signal (i.e., delay spread and power delay profile). Literature shows that there are a wide range of works that characterise the channel using UWB measurements [8]–[10]. These works obtain statistical propagation models from the experimental results. However, measurement campaigns are usually time-consuming requiring dedicated material and human resources. As alternative, deterministic methods [11]–[13] based on numerical approaches which involve either solution of Maxwell's equations using full-wave simulation techniques or geometrical approximations such as Ray Launching (RL) [14] and Ray Tracing (RT) [15] can be employed. In principle, these techniques generate more precise results but require higher computational demands than statistical techniques. Another advantage in the use of deterministic methods is the possibility of using the available floor plan to generate a detailed information of the topology of the environment. This can be useful in providing more insights on the impact of several properties within the environment under analysis. In this sense, the use of deterministic based models, such as RT or RL enable precise characterization in terms of time domain properties as well as RF power level estimations, when compared with empirical/statistical based models. Time domain components can be evaluated at an individual component level as well as in ray beams. Indoor impact can be carefully determined, considering non-uniform topological scatterer distributions, as well as cluster configurations.

Despite the advantages of deterministic methods, to the author's knowledge, few references [36]–[41] briefly analyze the UWB channel using RL or RT techniques i.e., focus on a specific characteristic of the UWB indoor multipath channel such as power delay profile [36]–[38] and path-loss [42]. In [39]–[41], RT techniques are somewhat proposed for UWB characterization, in order to derive time domain characteristics, RF power estimations or excess delay characterization in indoor scenarios, considering indoor structural configuration (i.e., walls, hallways, simplified furnishing models). The results obtained provide higher accuracy, particularly when considering site specific conditions within the scenarios under analysis. However, complex clutter distributions or combined time-frequency analysis approaches have not been proposed. A possible reason for these few references is that back in the early 2000's when research on UWB was starting out, the use of deterministic techniques was more limited owing to high computational cost. Currently, UWB is being progressively adopted, thanks to multiple application domains, as previously stated. Additionally, computers exhibit higher computational capacity thanks to parallel-based computation, use of graphic processor acceleration or distributed computing architectures.

Research gaps which this work seeks to address include: a careful analysis the UWB channel using RL techniques. In the literature, we can find several works on UWB propagation models, applications and characterisation such as in Table 1. However, as far as the authors are concerned there is no work in the literature that provides a careful analysis of the UWB channel using 3D RL tool focusing on RF power levels as well as on time of flight (TOF) estimation.

In this paper, not only do we present a novel analysis of the UWB channel using an inhouse developed 3D RL, but also use the RL technique to obtain the accurate ranging results from the time domain properties of the signal. Accuracy of the results is shown by comparing simulation vs measurements in several spatial points of the scenario. Therefore, the specific contribution of this paper is three fold:

1) The UWB propagation channel is modelled in an indoor environment using an accurate 3D RL tool.
2) The convergence of the developed 3D RL tool is studied with respect to the size of the cuboid.
3) Using the time domain properties of the UWB signal, the 3D RL tool is used to obtain the accurate TOF ranging results which can be used in any positioning application.

The structure of the remainder of this paper is as follows. Section II presents the theory behind the analysis of radio signals using 3D RL tool. The inhouse developed 3D RL code is analytically described and validated using a set of measurements in section III. The statistical UWB models is presented in section IV. In section V, the estimation of position related parameters such as the range is presented. Finally, in the last section, conclusions are given.

II. RAY LAUNCHING ANALYSIS

Previously in the 1990s, RL and RT were together categorised as RT techniques. More recently, however, the distinctions have been made clearer. In the RL approach, the Tx sends thousands of rays in a solid angle and the algorithm follows the propagation of each ray until it either arrives at the Rx or becomes so weak to be significant. In RT, the rays are traced from the principal radio wave propagation regions that are estimated.

The majority of the works on RL or RT techniques in the scientific literature focus on narrow band channel measurements and modelling for office indoor scenario [43], public transportation buses [44], vehicular [45], aircraft [46], and metro environments [47]. These works utilise the conventional RL. However in systems where the signal occupies a

TABLE 1. UWB propagation model/application and characterisation.

Ref	Channel Model/Application	Characteristic
[16]	UWB Personal Area Networks Propagation	Description of 802.15.3a channel model, including aspects such as path loss, fading and time variance
[17]	UWB Indoor Propagation Model Overview	Description of time domain and frequency domain models for different indoor environments, with distance ranges from 1-20m
[18]	Time Domain Channel Model in 3.6GHz-6GHz Band	UWB Channel Sounding is performed, by applying a carrier frequency modulated by a train of PN shaped pulses
[19]	Underground Tunnel UWB Propagation	Inverse Ray Method is applied in order to perform model fitting in an underground mine scenario
[20]	Body Area Network propagation model overview	Description of narrowband and ultra wideband channel models and discussion on multiple model statistics and effects in the case of considering wearable devices and conditions
[21]	Effect of Antenna Characteristics in On Body Indoor Environments	Characterization of different parameters such as time delay profile, path loss and RMS delay spread are presented for different on body antenna locations, considering tapered slot antennas and planar inverted cone antennas.
[22]	UWB Signal Characterization in Military Airplanes	Channel Transfer Function is extracted from measurements within an indoor C-130 military airplane
[23]	Characterization of Clusters in UWB in Home Environments	Parameter extraction based on double directional channel sounder measurements in wooden indoor home environments
[24]	Beam Tracing Site Specific Indoor UWB Channel model	An indoor propagation model based on pyramidal beam tracing model is presented. The model is tested in LOS and NLOS conditions
[25]	Propagation of UWB signals in the human head	Propagation phenomena such as reflection, refraction, diffraction and surface wave propagation are analyzed from 1.5 GHz to 8 GHz, focusing on ear to ear propagation, observing strong attenuation effects.
[26]	UWB Massive MIMO Performance Analysis	A Ray Based procedure is employed in order to obtain optimal spatial separation values of antenna elements under favorable propagation conditions in massive MIMO systems.
[27]	UWB Propagation Characterization in Human Chest	Human body propagation is analyzed, specifically in the case of the chest, by voxel electromagnetic simulation, in LOS conditions in the 100MHz to the 5 GHz range.
[28]	UWB Wireless Operation of Endoscopy Capsules	Evaluation of performance in terms of wireless channel analysis and temperature profile of wireless endoscopy capsules with integrated UWB transceiver devices, in the 3.5GHz to 4.5GHz
[29]	UWB On Body Channel model considering different body postures	UWB wireless channel models are obtained by full wave FDTD simulation, considering a human body model implementing different postures and with different transceiver links.
[30]–[34]	Human Body shadowing effect in UWB ranging pedestrian tracking	Error within ranging algorithms applied for pedestrian location tracking owing to losses given by human body are modeled in the 4GHz UWB band. The results are later applied in order to minimize overall ranging errors, improving UWB tracking estimation precision.
[35]	Wireless Channel characterization for telemetry applications in transplanted organ monitoring	Wireless channel characterization is presented in the 4.5GHz-6.5GHz range, applied to telemetry in implanted transceivers for transplanted organs. The specific case of liver transplant is considered, exhibiting an attenuation range in the 50dB-100dB. Respiratory movement effect have also been characterized in terms of path loss estimation.

wide bandwidth such as in UWB, a sub-band divided RL technique (i.e., simulating the channel at multiple center frequencies of the corresponding sub-bands) is recommended.

A. CONVENTIONAL RAY LAUNCHING

An inhouse implemented 3D-RL algorithm has been used for the UWB channel characterization. The developed algorithm is based on the conventional RL approach centred on the shooting and bouncing rays (SBR) technique, where a set of rays are launched from the Tx in a solid angle predefined as input parameter. The algorithm is based on Geometrical Optics (GO) and the Uniform Theory of Diffraction (UTD). GO can be seen as an asymptotic solution of Maxwell's equations and has proved to be precise in propagation prediction problems if the dimensions of the obstacles are large enough compared to the wavelength [48]. However, GO can lead to uncertainties in shadow regions where diffraction has higher impact, so it needs to be completed with the UTD to achieve accurate results in complex environments where a high quantity of obstacles is encountered [49], [50]. Thus, the combination of GO and UTD is an appropriate solution to model radio wave propagation provided the geometry and the scenario details, where an exact solution of Maxwell's equations could be unaffordable to compute.

The inhouse developed 3D-RL algorithm considers the morphology and topology of the scenario, as well as all the obstacles within it, by means of a realistic 3D recreation of the environment. Parameters such as number of reflections, radiation pattern of the transmitter and receiver antennae, angular resolution of launching rays and spatial resolution of cuboids size are considered as input parameters. The algorithm has been validated in the literature for propagation prediction at complex indoor environments, achieving a good trade-off between results accuracy and computational load [51]. In order to decrease computational load with a slightly decrease in precision, it can also be hybridized with other approaches, such as neural networks [52], collaborative filtering [53] or electromagnetic diffusion equation [43]. These hybrid approaches can be used depending of the complexity of the scenario and the expected results accuracy, which could serve for different radio planning engineering purposes.

B. SUB-BAND DIVIDED RAY LAUNCHING

Given the inherently large bandwidth of operation, the UWB propagation channel is frequency selective. Hence, channel charactersitics may vary considerably over the entire UWB bandwidth. Therefore, it is not enough to simulate UWB systems using the conventional RL technique applied to one discrete frequency. Overcoming this challenge requires use of a sub-band RL that has been already applied to works in [36] and [38]. The basic idea is simulating the UWB channel at multiple center frequencies of the corresponding sub-bands. We summarise sub-band divided RL into the following:

1) The entire bandwidth is split into several sub-bands where a constant frequency characteristic for materials can be assumed. The higher the number of sub bands the more accurate the algorithm, but at a higher computational cost.
2) At each center frequency, the conventional RL is deployed to extract the channel impulse response (CIR).
3) A complete frequency response over the entire UWB bandwidth is obtained by combining all the frequency responses from all the sub-bands.

Each UWB radio channel can have a bandwidth of more than 500 MHz, depending on its centre frequency. In our work, we shall consider 4 GHz as the primary frequency of interest and a bandwidth of 500 MHz because: (i) several UWB commercial systems for positioning are available at this frequency, and (ii) the bandwidth of 500 MHz has been shown to be sufficient in obtaining accurate TOF results [54]. Using the Sub-band Divided RL technique, the frequency bandwidth of 500 MHz is thus divided into two sub-bands with 250 MHz each i.e., RL simulations and measurements are performed at 3.75 GHz, 4 GHz, and 4.25 GHz.

III. RAY LAUNCHING SIMULATION ALGORITHM

In order to calibrate the simulation scenario under test, a preliminary and simple experiment was performed to determine the frequency selectivity of the UWB channel at the considered frequencies. The Tx employed was a Hewlett Packward 8753D (30 KHz – 6 GHz) signal generator, where as the Rx was a portable Agilent N9912 Field Fox spectrum analyzer, with 100 MHz bandwidth directly connected via a coaxial transmission line. Rx bandwidth has been selected in order to increase signal to noise ratio and hence detection capabilites. This is feasible owing to the fact that the 3D RL sub band simulations are based on a continuous wave approach.

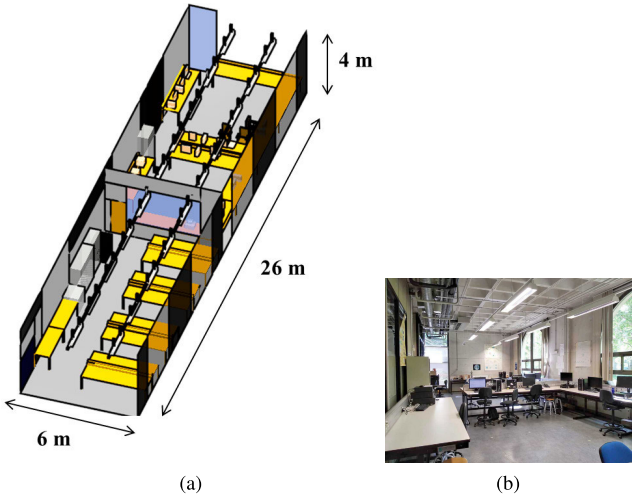

FIGURE 1. Description of the scenario: a) Schematic by the 3D RL tool and (b) details of the Luis Mercader Lab environment. There is a glass wall at the length of 15m separating the two rooms of the Lab.

The Tx power of the signal generator was set at maximum of 10 dBm. The measured RF power at 3.75, 4 GHz and 4.25 GHz were 7.5 dBm and 7 dBm, respectively, which indicating that the respective cable and connector losses accounted for 2.5 dB and 3 dB.

Simulations of a typical lab indoor scenario which is located at department of Electric, Electronic and Communication engineering of the Public University of Navarra in Spain was then performed. The dimensions of the scenario were $26 \times 6 \times 4\ m^3$. The schematic view in Figure 1 shows all the interacting objects (IOs) such as walls, computers, monitors, chairs, desks, closets within the scenario and have been taken into account in the simulation process. In addition, material properties of the objects as defined by their dielectric constant and permittivity in Table 2, as well as propagation phenomena like reflection, diffraction or refraction have all been taken in account. The parameters for all of the materials included in the scenario, as provided in [55] are given in the 1 GHz - 10 GHz frequency, valid for the UWB frequency range under consideration.

During the simulation, other parameters such as frequency of operation, the angular and spatial resolution, the maximum number of permitted rebounds (the number of interactions between a propagated ray and the obstacles), the angular and spatial resolution, antenna type and gain, transmission power level have been considered according to Table 3. These parameters have been chosen to achieve adequate accuracy and optimization of the simulation results.

FIGURE 2. Upper view of the created scenario. The red dashed line corresponds to the measurement points.

TABLE 2. Material properties for 3D RL simulations [55].

Material	ϵ_r	Conductivity (S/m)
Air	1	0
Brick wall	4.44	0.11
Wood	2.88	0.21
Plasterboard	2.02	0
Aluminium	4.5	37.8×10^6
Doors	5.84	0.06
Polypropylene	3	0.11
Concrete	8.5	0.02
Glass	6.06	0.11

TABLE 3. 3D RL simulation parameters.

Parameter	Value
Operation Frequency	3.75 / 4 / 4.25 GHz
Antenna Type	Monopole
Antenna Gain	0 dBi
Transmitted Power	10 dBm
Cuboid size (Mesh resolution)	From 0.1 to 0.9m
Launched rays angular resolution	1 degree
Permitted maximum rebounds	6
Diffraction phenomenon	Activated

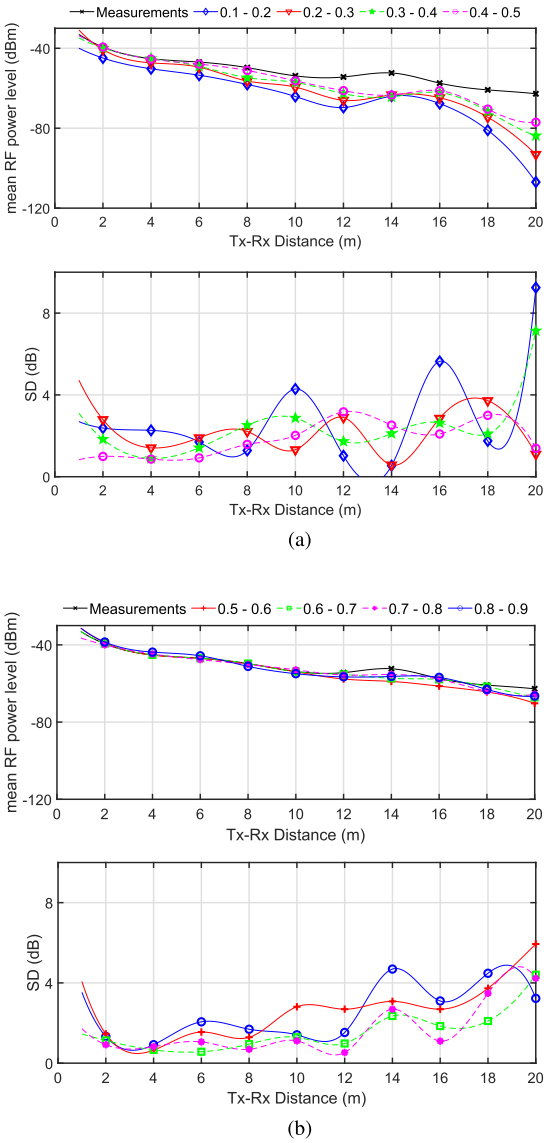

FIGURE 3. The comparison between the 3D RL simulation results and real measurements at 4 GHz for cuboid size intervals: (a) from 0.1 to 0.5 m, and (b) from 0.5 to 0.9 m. The mean RF power level and standard deviation (SD) are obtained from the averaging the RF power from the possible fixed cuboid sizes within the respective cuboid size interval. Results for 3.75GHz and 4.25GHz follow a similar trend.

The 3D scenario in Figure 1 is designed as a structure made up of a matrix of fixed cuboids whose size has been varied according to Table 3. Essentially as a ray is sent from the Tx at the coordinates (x = 4.1 m, y = 1.47 m, z = 1.60 m) [see – Figure 2] through or to a given cuboid, its propagation parameters are stored in the corresponding matrix that represents the cuboid. Hence, it is possible to obtain the RF power from each cuboid for analysis as illustrated in Figure 3. Note that the RF power levels are obtained from the same spatial locations for both the measurements and simulations (obtained from 3D mesh of cuboids in which the scenario has been divided).

A. TEST SCENARIO VALIDATION

Validation of the RL simulation method was achieved by conducting measurements within the simulated scenario at the considered UWB frequencies. The Tx and Rx antennas were connected to the signal generator and portable spectrum analyzer, respectively through coaxial cables. Both Tx and Rx antennas were omnidirectional UWB Partron dielectric chip 0 dBi gain antenna manufactured by Abracon. Similar to the simulations, the Tx has been located at the coordinates (x = 4.1 m, y = 1.47 m, z = 1.60 m) as depicted in Figure 2. Measurements were performed along the dashed line also depicted in Figure 1 at a height of 1.6 m, with a spacing of 2 m between the points. At each point, the measurements were conducted for a duration of 60 s so that the maximum RF power level is obtained within the given time span and measurement bandwidth. The results of the test scenario validation are illustrated in Figure 3 and Figure 5.

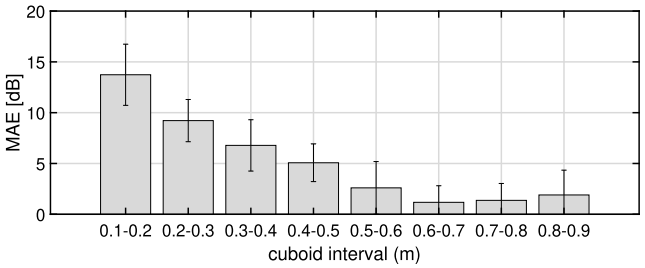

FIGURE 4. Mean absolute error (MAE) at different cuboid size intervals. The error bars is the SD. The MAE is obtained from averaging the error obtained from RF power results in Figure 3.

B. RF POWER CONVERGENCE VERSUS THE CUBOID SIZE

One of the most relevant aspects of RL simulations is defining the appropriate 3-D cuboid mesh to obtain accurate results. As a result, convergence analysis was performed to find the optimal cuboid resolution needed to obtain accurate RF power estimations when modelling the UWB radio wave propagation channel in this environment. For every interval, eight different fixed cuboids sizes are considered and analysed i.e., the analysis considered both cubes and cuboids. In Figure 3 we show the mean and the SD of the RF power at 4 GHz obtained from the simulations versus the measured RF power. The estimated RF power becomes more accurate as the cuboid size intervals increase and converges at the interval $0.6-0.7$ as seen in Figure 4. This implies that the maximum accuracy of the algorithm is reached when simulations are made within this cuboid size interval. A further assessment of the $0.6-0.7$ interval shows that the cuboid size of 0.6/0.6/0.6 (0.6 m cuboids resolution in the x, y, z dimensions) in particular provides relatively accurate results. This is clearly evident in Figure 5 where a comparison between the measured and simulated Rx power is made. Looking at Figure 5, the first observation is that all results fit with the measured RF power trend curve, i.e., the power decaying with increasing Tx–Rx distance. The results also show that there exists a clear fit in the trends of the measured and simulated curves, which validates the algorithm. In fact in Table 4 the mean error and SD at the corresponding frequency of interest are shown. Most of the errors observed are mainly due to approximations made in simulation. Note that due to the relatively small differences in the RF power between the simulations and measurements, the analysis in respect to the RF power for the rest of this paper has been made with reference to the aforementioned cuboid size.

C. BI-DIMENSIONAL RF POWER DISTRIBUTION

The presented inhouse developed RL simulation tool provides 3D results, i.e., estimations for the complete volume of the analyzed environments are obtained. As an example, Figure 6 shows the bi-dimensional RF power distribution planes within the current scenario under analysis for different heights: from 0m to 0.6m, 1.2m to 1.8m (the transmitter location height) and 3m to 3.6m. Tx location is depicted by a red circle. The three height planes are shown for the chosen

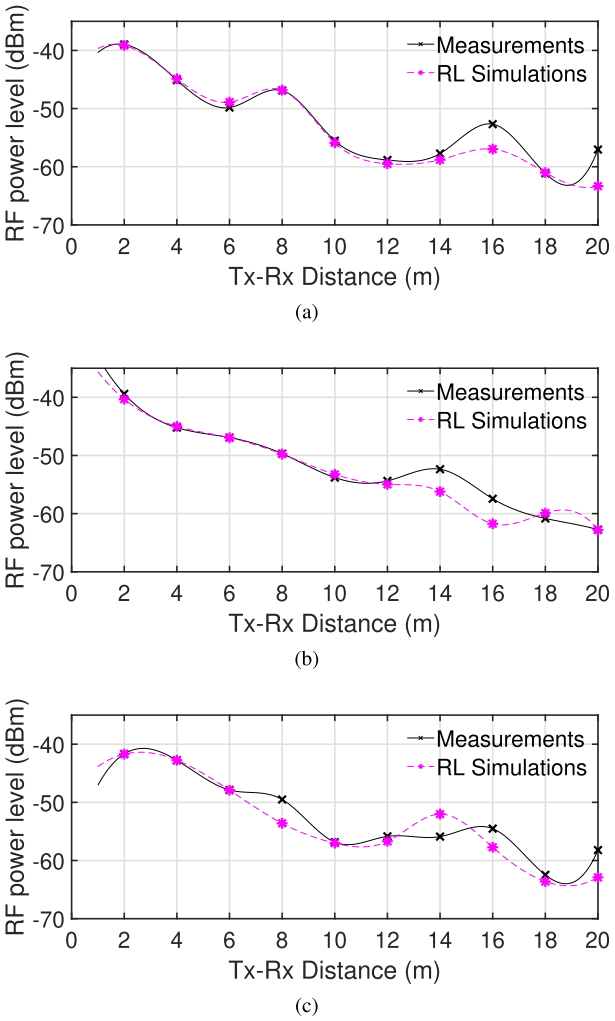

FIGURE 5. The comparison between the 3D RL simulation results and real measurements for the center frequencies: (a) 3.75 GHz, (b) 4 GHz, and (c) 4.25 GHz at the cuboid size of 0.6/0.6/0.6.

TABLE 4. Comparison between the 3D RL simulation results and real measurements.

Frequency (GHz)	Mean Error [dB]	SD [dB]
3.75	1.42	2.12
4	1.15	1.57
4.25	1.81	1.92

three operation frequencies: 3.75 GHz, 4 GHz and 4.25 GHz. It is worth noting that the obtained results show the typical rapid RF power variations of an indoor environment where the multipath propagation phenomenon has a big impact. At first glance, the differences between the heights can be clearly seen.

But on the other hand, the results between different operation frequencies seem quite similar. In order to gain insight in this, in Figure 7 RF power level difference planes are presented. Specifically, Figure 7 shows the difference between 3.75 GHz and 4.25 GHz results at 1.2-1.8m height (left) and

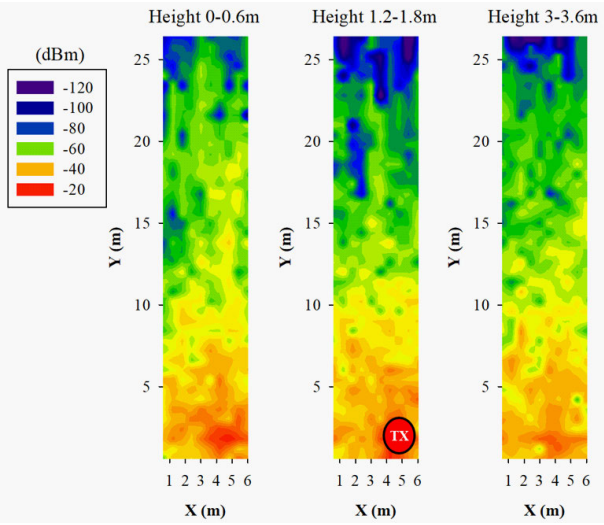

(a)

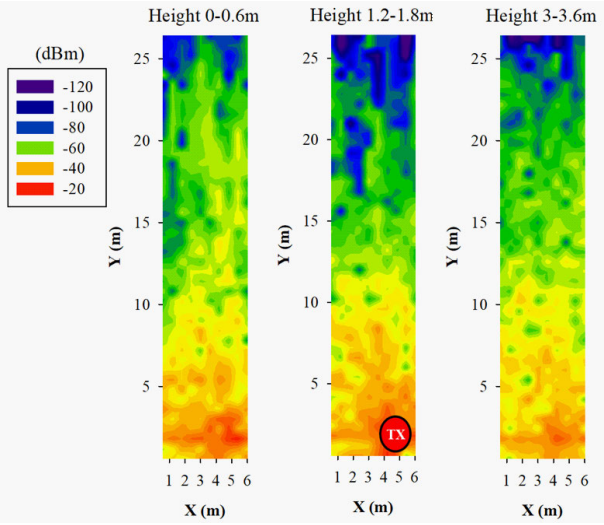

(b)

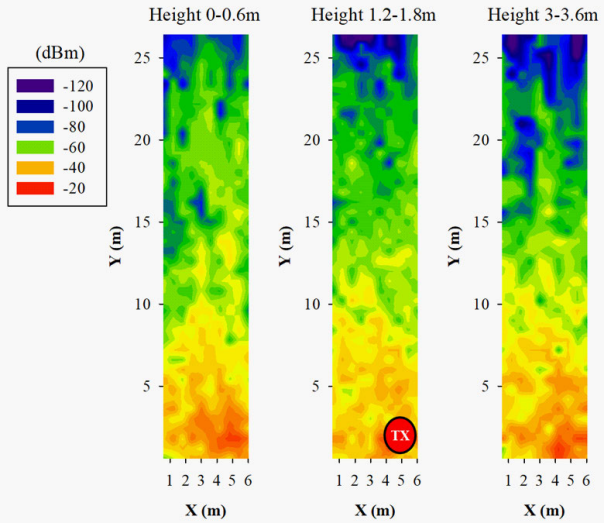

(c)

FIGURE 6. Bi-dimensional RF power distribution planes for different heights. (a) at 3.75 GHz, (b) 4 GHz, (c) 4.25 GHz.

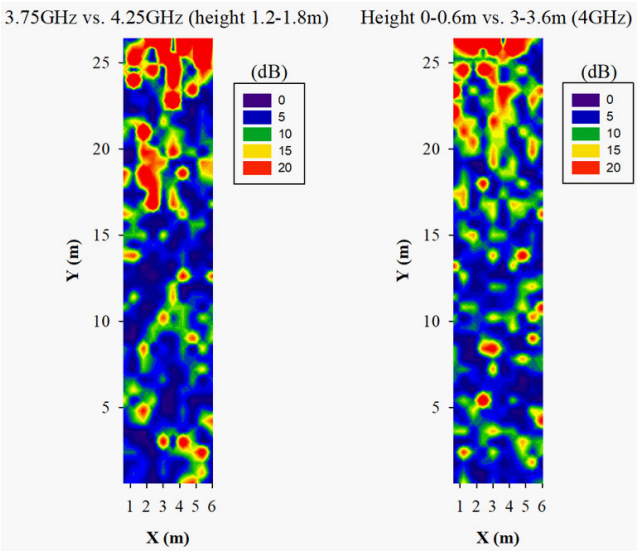

FIGURE 7. Bi-dimensional RF power distribution planes difference between operation frequencies (left) and heights (right).

the difference between height 0-0.6m and 3-3.6m at 4 GHz (right). These results show that the RF power level can be as high as 20 dB (or more) in some points and zones of the scenario under analysis. This reinforces the idea of following the presented sub-band divided RL methodology when communication technologies such as UWB are employed, where the bandwidth is much wider than other common wireless communication systems (such as WiFi or ZigBee), exhibiting frequency dependent characteristics.

IV. STATISTICAL UWB CHANNEL MODELS

Once that 3D-RL simulation methodology has been validated, propagation characterization is described in this section. We will focus on the following primary characteristics of indoor multipath channel: i) path-loss, (ii) small scale fading, and (iii) power delay profile.

A. PATH-LOSS ANALYSIS

The path loss models can be used to estimate link budgets, capacity, cell sizes and shapes, etc. Generally, the path loss model in UWB systems is not only dependent on distance like narrow band systems, but also on the frequency and bandwidth [8].

Initially, the friis free space model (narrow band model), which includes effects of the Tx and Rx antenna can be used as good approximation for the path loss analysis. However, as it is stated in the final report of the IEEE 802.15.4a UWB channel model [56], the specific antennas used for each case will have different specifications, and therefore, a model that only describes the wireless channel is presented in (1)

$$PL(f) = \frac{P(f)_r}{P(f)_t} \tag{1}$$

$$PL(f) = \frac{1}{2}.PL_0.\eta_t.\eta_r.\frac{(\frac{f}{f_c})^{-2.(k+1)}}{(\frac{d}{d_0})^n} \tag{2}$$

where PL_0 is the path-loss at $1m$ distance, f is the bandwidth of the model (2-10 GHz), $P(f)_r$ is the RF power level, $P(f)_t$ is the Tx power level, $PL(f)$ is the path-loss defined in (2), f_c is the central frequency, d is the distance, d_0 is the reference distance (1m), n is the pathloss exponent, k is the frequency dependence of the path-loss of the model, and η_t and η_r are efficiencies of the Tx and Rx antennas respectively. This model can be consulted in Section III of [56], in which UWB Model parameterization for 2-10 GHz is made under the Residential, Indoor office, Outdoor, Open outdoor and Industrial environments.

Taking into account the morphological characteristics of the scenario under analysis in this work, the Indoor office environment model has been chosen in order to compare it with the 3D RL simulation results. The comparison is presented in Figure 8, for 3.75 GHz, 4 GHz and 4.25 GHz frequencies.

The results presented show that the 3D RL results follow the tendency marked by the IEEE 802.15.4a channel model for indoor office environments. It is worth noting that the obtained RF estimations start following the LoS line and by increasing the distance from the Tx the values change the tendency and follow the NLoS curve (at 15m approximately), which is due to the obstacles and elements that appear in the line of sight (e.g. a door, the glass wall, etc. [see – Fig. 1]).

B. SMALL SCALE FADING

Small scale fading is the fluctuation of power over very short periods of time caused by interference between multipath components. It is usually modelled as different distributions such as Gamma, Lognormal, Rician, Rayleigh, Nakagami, Weibull, or mixture between them [57].

Figure 9 presents the simulated cumulative distribution function (CDF) of the RF power for the respective frequency in the considered scenario along the linear distribution line in front of the Tx antenna. The comparison with the theoretical distributions which best fits the simulated data has been also presented. To measure the closeness of the data with the theoretical distributions, the Anderson-Darling (AD) goodness-of-fit (GOF) test with 5.0% for the significance level of the hypothesis (Ho) test has been used [58]. Table 5 presents the AD statistic results for the fitted distributions for the three considered frequencies (i.e., 3.75, 4 and 4.25 GHz), with the hypothesis result, p-value, AD statistic and squared coefficient value (SCV). The SCV is a measure of the data variability. Indeed, the SCV characterizes the amount of fading of the RF signal power [59]. It can be observed that the Lognormal and Weibull distributions are the best fits for this specific scenario for the three considered frequencies, where the test fails to reject the null hypothesis at the default 5% significance level.

C. POWER DELAY PROFILES

To gain insight into the small-scale variation in specific spatial locations of the scenario, the multipath variations has been analyzed with the power delay profile (PDP) for a specific spatial sample where high multipath is obtained. For that purpose, the CDF of a power delay profile at a point located at 5 meters distance in front of the Tx antenna has

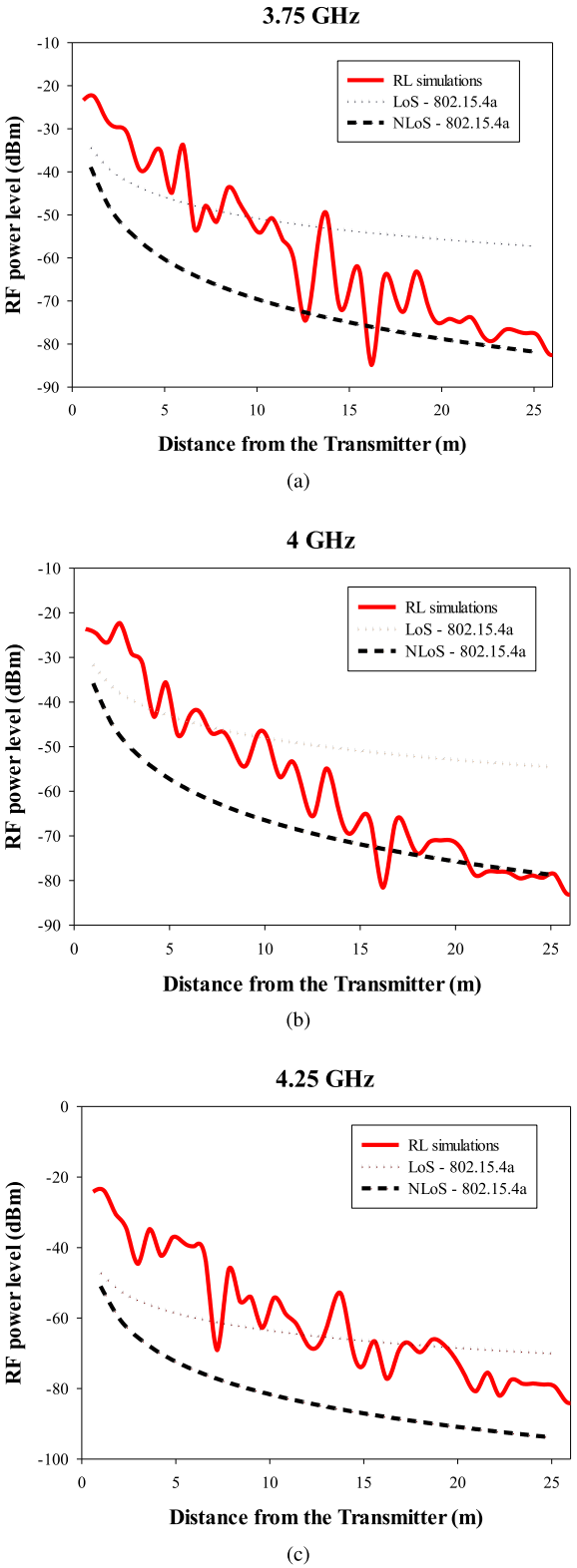

FIGURE 8. Comparison between 3D RL simulation results and the Indoor office environment of 802.15.4a channel model, a) at 3.75 GHz, b) 4 GHz and c) 4.25 GHz. The results correspond to the linear path highlighted in Figure 2.

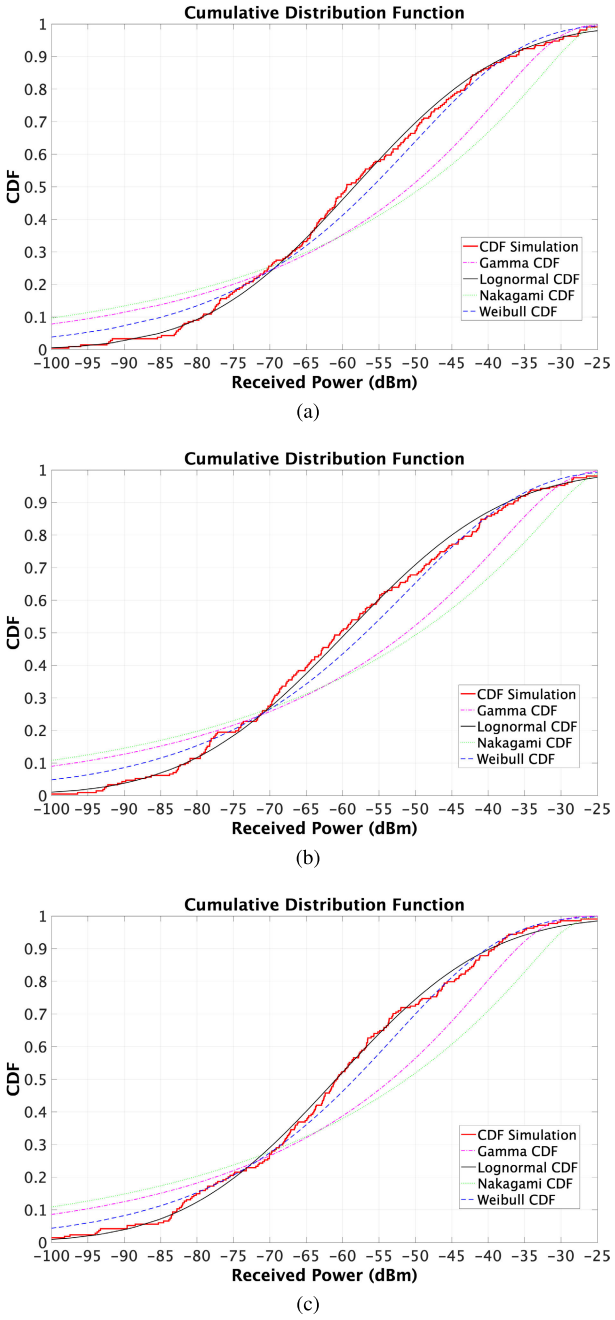

FIGURE 9. CDF of RF power along the linear distribution line in front of the Tx and comparison with theoretical distributions: (a) 3.75 GHz, (b) 4 GHz, and (c) 4.25 GHz.

been computed and compared against Rayleigh distribution, which is commonly used to describe multipath statistics for narrowband channels at indoor environments [57].

The probability density function (PDF) of a Rayleigh distributed random variable is given by (3)

$$p(r) = \frac{r}{\sigma^2} e^{-\frac{r^2}{\sigma^2}} \tag{3}$$

where r is the magnitude of the RF power, and σ is the SD of the multipath propagation. The CDF of Rayleigh distribution is obtained via integration over the PDF and is presented in

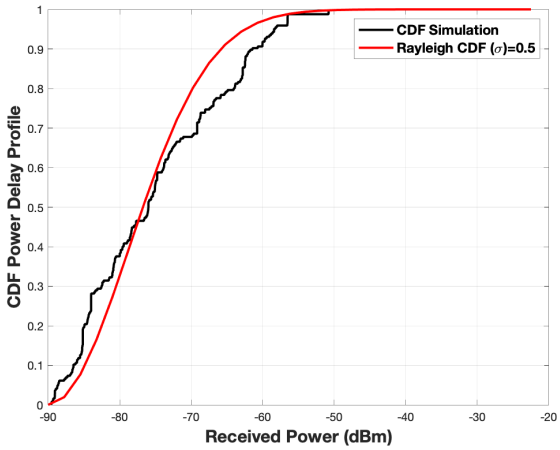

FIGURE 10. CDF of the PDP for a spatial point located at 5 m in front of the Tx antenna, and comparison with Rayleigh distribution.

Figure 10. It is observed a good fit with Rayleigh distribution with $\sigma = 0.5$.

V. ESTIMATION OF POSITION-RELATED PARAMETERS

Since a key application of UWB systems is positioning using TOF measurements, in this section, we provide an analysis of how 3D RL results can be tailored for ranging applications. Firstly, we perform extensive RL simulations to extract the TOF from the signals. Secondly, we carry out TOF measurements using commercial available UWB nodes to validate the simulations.

A. RAY LAUNCHING TOF SIMULATIONS

Estimation of TOF results is given by analyzing the ray path and considering propagated component, given by the cuboid simulation grid. The results are obtained by considering detection of ray components by surface detection of impinging rays, as a function of the direction of arrival of the rays launched.

In this way, depending on the relative locations of transceivers within the scenario, there is a deviation range in the detected components, exhibiting an average variation defined in (4).

$$D = \frac{\sqrt{3} d_{cuboid}}{2} \tag{4}$$

where d_{cuboid} is the cuboid edge dimension, given a uniform cubic lattice mesh, as depicted schematically in Figure 11. These variations are function of the cuboid location and the relative locations of Tx source and Rx observations point, as this will condition both the ray distribution (i.e., location of impinging ray/surface location) and the reference for subsequent distance estimation, which leads to larger variations the larger the cuboid edge size is in the mesh.

The average variations for different cuboid sizes and different observation frequencies are depicted in Figure 12, for the set of simulation results obtained in Table 6. Looking at Figure 12, it can be seen that average variations increase as cuboid sizes increase, consistent with larger value of D as defined in (4) and hence, larger impact surface of the

TABLE 5. RF power Anderson-Darling test statistics.

Distribution	Lognormal	Gamma	Nakagami	Weibull
		Frequency =3.75GHz		
Hypothesis	0	1	1	0
p_value	0.94	$2.8e^{-06}$	$2.8e^{-06}$	0.09
AD statistic	0.28	12.57	18.85	2.01
SCV	2.49	2.49	2.49	2.49
		Frequency = 4 GHz		
Hypothesis	0	1	1	0
p_value	0.71	$2.8e^{-06}$	$2.8e^{-06}$	0.06
AD statistic	0.52	12.37	18.49	2.23
SCV	2.49	2.49	2.49	2.49
		Frequency = 4.25 GHz		
Hypothesis	0	1	1	0
p_value	0.73	2.8e-06	2.8 -06	0.14
AD statistic	0.51	11.72	20.30	1.65
SCV	2.49	2.49	2.49	2.49

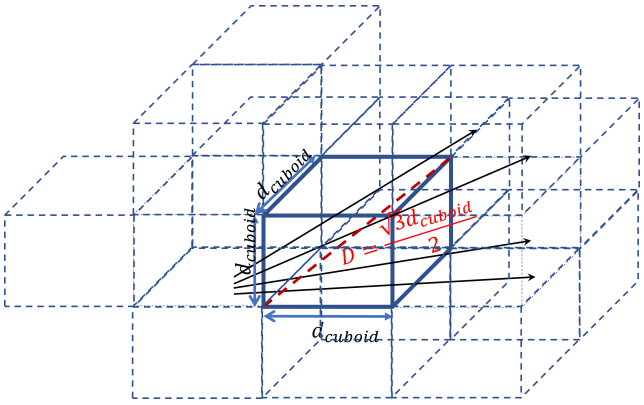

FIGURE 11. Schematic representation of distribution of volumetric launched rays within the simulation grid, in which ray detection is determined by impinging ray surface.

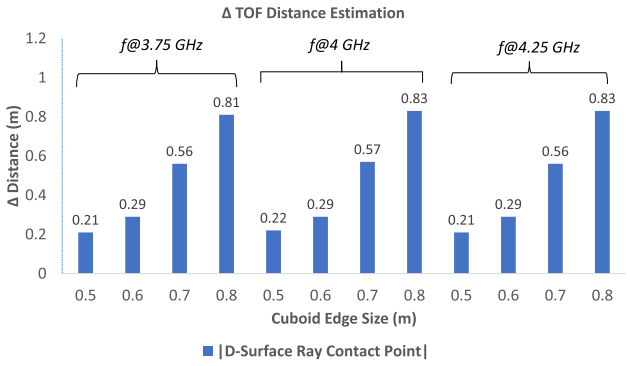

FIGURE 12. Variation in TOF distance estimation, as a function of cuboid size and frequency under consideration.

impinging rays within the cuboid under analysis. These variations are all below the corresponding average geometrical limits given by D as a function of the cuboid size and can subsequently error in TOF estimation can be reduced by adequate post-processing.

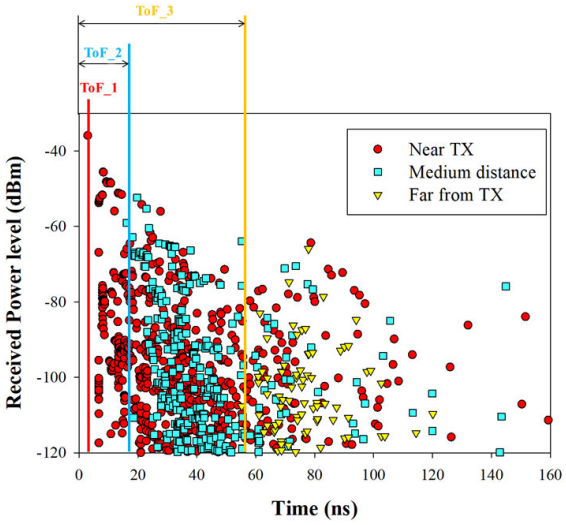

FIGURE 13. PDP comparison among 3 locations at 1.6 m height for different distances from the Tx.

B. EXTRACTION OF TOF RESULTS

According to Molisch [9], the delay dispersion has a great impact on the performance of ranging devices. Therefore, in this paper, the TOF in Table 6 is extracted by detecting the first path of the signal (obtained from the PDP) for each of the locations along the straight path [see – Fig. 13]. In fact, Figure 13 shows 3 diffferent PDPs obtained by the 3D RL algorithm. This graph shows the amount of launched rays that reach 3 different locations within the scenario under analysis. The red dots correspond to a location close to the Tx antenna, the yellow triangles correspond to a point far from the Tx, and the blue squares to a midpoint distance. Each colored unit shows the information (RF power level and the arrival time) of each of the received rays at a specific location. As expected, the environment is very rich in terms of multipath propagation phenomenon, i.e., a lot of multipath

TABLE 6. Summary of the simulation versus real distance (R) at different cuboid intervals and UWB center frequencies in GHz (F). For each cuboid interval (C), eight combinations of the fixed cuboid sizes were simulated. In this table, we show the mean and SD of the simulated distances in metres.

F	C \ R	2	4	6	8	10	12	14	16	18	20
3.75	0.1 - 0.2	3.2± 0.1	4.7± 0.1	6.6± 0.1	8.2± 0.4	10.1± 0.1	12.0 ± 0.1	14.0 ± 0.2	16.5± 0.0	18.5± 0.1	21.0± 0.2
	0.2 - 0.3	2.9± 0.3	4.5± 0.1	6.2± 0.3	8.0± 0.0	10.0± 0.1	11.8 ± 0.4	14.2 ± 0.2	16.1± 0.2	18.1± 0.2	20.6± 0.3
	0.3 - 0.4	2.3± 0.3	4.1± 0.1	6.0± 0.1	8.0± 0.1	10.0± 0.1	11.6 ± 0.3	14.0 ± 0.2	16.0± 0.1	18.1± 0.1	20.1± 0.2
	0.4 - 0.5	2.1± 0.1	4.0± 0.1	6.0± 0.1	8.0± 0.2	9.7± 0.3	11.4± 0.1	13.9± 0.2	16.1± 0.1	18.0± 0.1	20.1± 0.1
	0.5 - 0.6	2.1± 0.1	4.0± 0.1	6.0± 0.2	7.9± 0.2	9.8± 0.2	11.3± 0.4	13.8± 0.2	16.0± 0.2	18.0± 0.1	20.1± 0.2
	0.6 - 0.7	2.0± 0.1	4.1± 0.1	5.9± 0.2	7.9± 0.1	9.7± 0.3	10.9± 0.6	13.6± 0.6	15.9± 0.5	17.8± 0.2	19.6± 0.3
	0.7 - 0.8	2.0± 0.1	4.0± 0.2	5.8± 0.3	7.5± 0.3	9.7± 0.4	10.9± 0.6	13.2± 0.4	15.3± 0.5	17.4± 0.3	19.3± 0.2
	0.8 - 0.9	2.0± 0.2	4.0± 0.2	5.8± 0.3	7.7± 0.3	9.7± 0.4	10.9± 0.6	13.2± 0.6	15.3± 0.3	17.2± 0.3	19.1± 0.2
4	0.1 - 0.2	3.2± 0.1	4.7± 0.1	6.6± 0.1	8.2± 0.4	10.1± 0.1	12.0 ± 0.1	14.0 ± 0.2	16.5± 0.0	18.5± 0.1	21.0± 0.2
	0.2 - 0.3	2.9± 0.3	4.5± 0.1	6.2± 0.3	8.0± 0.0	10.0± 0.1	11.8 ± 0.4	14.2 ± 0.2	16.1± 0.2	18.1± 0.2	20.6± 0.3
	0.3 - 0.4	2.3± 0.3	4.1± 0.1	6.0± 0.1	8.0± 0.1	10.0± 0.1	11.6 ± 0.3	14.0 ± 0.2	16.0± 0.1	18.1± 0.1	20.1± 0.2
	0.4 - 0.5	2.0± 0.1	4.0± 0.1	6.0± 0.1	8.0± 0.2	9.7± 0.3	11.4± 0.1	13.9± 0.2	16.1± 0.1	18.0± 0.1	20.1± 0.1
	0.5 - 0.6	2.1± 0.1	4.0± 0.1	6.0± 0.2	7.9± 0.2	9.8± 0.2	11.3± 0.4	13.8± 0.2	16.0± 0.2	18.0± 0.1	20.1± 0.2
	0.6 - 0.7	2.0± 0.1	4.1± 0.1	5.9± 0.2	7.9± 0.1	9.6± 0.3	10.9± 0.6	13.6± 0.6	15.9± 0.5	17.8± 0.2	19.6± 0.3
	0.7 - 0.8	2.0± 0.1	4.0± 0.2	5.8± 0.3	7.5± 0.3	9.7± 0.3	10.9± 0.4	13.2± 0.6	15.3± 0.5	17.4± 0.3	19.3± 0.2
	0.8 - 0.9	2.0± 0.2	4.0± 0.2	5.8± 0.3	7.7± 0.3	9.7± 0.3	10.9± 0.4	13.2± 0.6	15.3± 0.3	17.2± 0.3	19.1± 0.2
4.25	0.1 - 0.2	3.2± 0.1	4.7± 0.1	6.6± 0.1	8.2± 0.4	10.1± 0.1	12.0 ± 0.1	14.0 ± 0.2	16.5± 0.0	18.5± 0.1	21.0± 0.2
	0.2 - 0.3	2.9± 0.3	4.5± 0.1	6.2± 0.3	8.0± 0.0	10.0± 0.1	11.8 ± 0.4	14.2 ± 0.2	16.1± 0.2	18.1± 0.2	20.6± 0.3
	0.3 - 0.4	2.3± 0.3	4.1± 0.1	6.0± 0.1	8.0± 0.1	10.0± 0.1	11.6 ± 0.3	14.0 ± 0.2	16.0± 0.1	18.1± 0.1	20.1± 0.2
	0.4 - 0.5	2.1± 0.1	4.0± 0.1	6.0± 0.1	8.0± 0.2	9.7± 0.3	11.4± 0.1	13.9± 0.2	16.1± 0.1	18.0± 0.1	20.1± 0.1
	0.5 - 0.6	2.1± 0.1	4.0± 0.1	6.0± 0.2	7.9± 0.2	9.8± 0.2	11.3± 0.4	13.8± 0.2	16.0± 0.2	18.0± 0.1	20.1± 0.2
	0.6 - 0.7	2.0± 0.1	4.1± 0.1	5.9± 0.2	7.9± 0.1	9.7± 0.3	10.9± 0.6	13.6± 0.6	15.9± 0.5	17.8± 0.2	19.6± 0.3
	0.7 - 0.8	2.0± 0.1	4.0± 0.2	5.8± 0.3	7.5± 0.3	9.7± 0.3	10.9± 0.4	13.2± 0.6	15.3± 0.5	17.4± 0.3	19.3± 0.2
	0.8 - 0.9	2.0± 0.2	4.0± 0.2	5.8± 0.3	7.7± 0.3	9.7± 0.3	10.9± 0.4	13.2± 0.6	15.3± 0.3	17.2± 0.3	19.1± 0.2

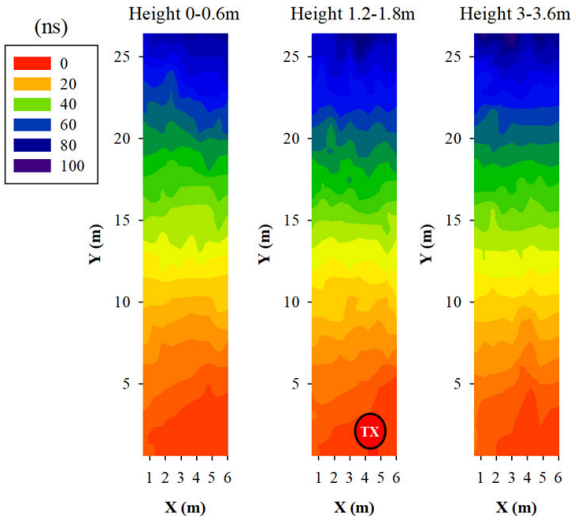

FIGURE 14. Bi-dimensional planes for the TOF simulation results.

components are present in the whole volume of the scenario. In addition, 3 vertical lines have been depicted in the graph in order to show graphically how the ToF has been obtained from simulation results. The vertical lines show the time the first ray needed to reach the specific location/cuboid within the scenario. This time is the estimated TOF.

Following this idea, Figure 14 presents bi-dimensional planes showing the estimated TOF for 3 different heights. As expected, the results are similar since the distance differences are small due to the reduced size of the scenario.

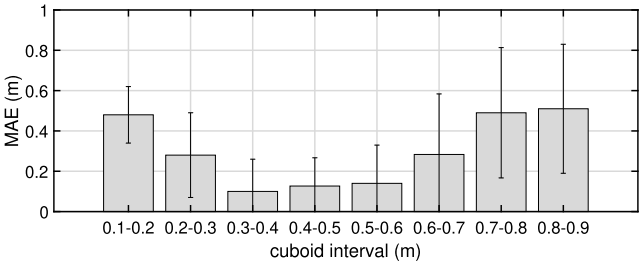

FIGURE 15. MAE at different cuboid size intervals. The error bars is the SD. The MAE is obtained from averaging the error obtained from TOF results in Table 6.

C. TOF CONVERGENCE VERSUS THE CUBOID SIZE

Similar to the RF power 3D RL simulations, a convergence analysis was performed to find the optimal cuboid resolution needed to obtain accurate TOF estimations. In Figure 6, the MAE at different cuboid size intervals is shown. Similar to work in Figure 4, the TOF range becomes more accurate as the cuboid size intervals increase and converges at the interval $0.3 - 0.4$, and then the error starts to increase afterwards. Therefore, it can be observed that 3D RL tool can be used to obtain decimetre level ranging accuracy as MAE of as low as 10 cm in Figure 15.

D. TOF MEASUREMENTS

Throughout this paper, we use two (one node configured as a Tx and the other as a Rx) TREK1000 development nodes manufactured by Decawave to measure the TOF of an UWB signal [54]. The nodes are fully compliant with the IEEE 802.15.4-2011 UWB standard, and are the best

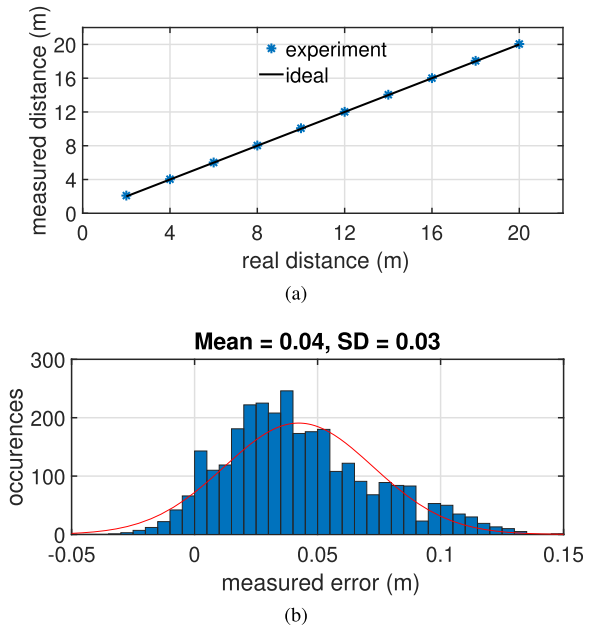

FIGURE 16. Indoor tests for TOF measurements: (a) real versus measured distances and (b) Histogram of distance error.

commercial products for TOF measurements [60]. For the purpose of this measurement campaign, nodes were configured to work with a 110 kb/s data rate and in the channel 2 (3990 MHz). The nodes operate in such a way that when a Tx sends a packet, the Rx hunts for the preamble or (once it has detected preamble) searches for start of frame delimiter (SFD) in the structure of the packet – which is the nominal point time-stamped by the IC. The 802.15.4 UWB standard requires that the time-stamp to be performed when the signal arrives at the antenna. Therefore, the Decawave Rx circuitry adds a correction factor determined by first path (leading edge) of the signal and also subtracts the Rx antenna delay to adjust the time stamp to the time at which the signal arrives at the antenna of the Rx.

A TOF measurement campaign was carried out in the Lab in Figure 1. The Tx was mounted on a mast at 1.6 m high at a fixed position. The Rx was also mounted on a tripod at the same height; however, it was moved from 2 to 20 m, with a 2-m step along a straight-path similar to dashed line in Figure 2. A laptop was connected to the Rx to store all measurements. At a rate of 3.57 Hz, TOF measurements were recorded over a period of 30 s, generating at-least 100 TOF estimations for each distance. The TOF results are multiplied by the speed of light to obtain the range and the results are in Figure 16.

The TOF ranging results are shown in Figure 16, in which the ideal ranges are compared with the experimental ones, as well as a histogram showing the number of occurrences for different range errors. As expected in Figure 16b, the range errors in LOS situations are modelled as a low-sigma Gaussian distribution. Looking at Figure 16, the mean error of up to 4 cm obtained during the measurements versus the 10 cm obtained during the simulations validates the 3D RL tool.

VI. CONCLUSIONS

We have presented a detailed analysis of the UWB channel for ranging applications using an inhouse developed 3D RL tool. RF power and TOF simulations have been performed in an indoor environment and validated using a set of measurements.

Using the sub-band divided RL technique, the UWB bandwidth of 500 MHz is divided into two sub-bands with 250 MHz each, therefore, RL simulations and measurements are made at 3.75 GHz, 4 GHz, and 4.25 GHz. A convergence analysis is performed which shows that adequate selection of the cuboid resolution is required to obtain accurate RF power and TOF results.

In addition, a detailed statistical UWB channel modelling is performed using the simulation results in terms of the path-loss, small scale fading, and PDP which are important when characterising an indoor radio channel. Therefore, similar to several narrowband systems, the 3D RL can be used as a valuable tool to test UWB systems for ranging applications with a mean accuracy of up to 10 cm in multipath conditions.

REFERENCES

[1] T. Mavridis, J. Sarrazin, L. Petrillo, P. De Doncker, and A. Benlarbi-Delai, "Information spatial focusing scheme for UWB wireless communications in smart environments," *IEEE Antennas Wireless Propag. Lett.*, vol. 14, pp. 20–23, 2015.
[2] Z. Wang, X. Xiao, H. Song, L. Wang, and Q. Li, "Development of anatomically realistic numerical breast phantoms based on T1- and T2-weighted MRIs for microwave breast cancer detection," *IEEE Antennas Wireless Propag. Lett.*, vol. 13, pp. 1757–1760, 2014.
[3] E. Pittella, S. Pisa, and M. Cavagnaro, "Breath activity monitoring with wearable UWB radars: Measurement and analysis of the pulses reflected by the human body," *IEEE Trans. Biomed. Eng.*, vol. 63, no. 7, pp. 1447–1454, Jul. 2016.
[4] C. Gimeno, D. Flandre, and D. Bol, "Analysis and specification of an IR-UWB transceiver for high-speed chip-to-chip communication in a server chassis," *IEEE Trans. Circuits Syst. I, Reg. Papers*, vol. 65, no. 6, pp. 2015–2023, Jun. 2018.
[5] Y. Xu, G. Tian, and X. Chen, "Enhancing INS/UWB integrated position estimation using federated EFIR filtering," *IEEE Access*, vol. 6, pp. 64461–64469, 2018.
[6] A. Yassin, Y. Nasser, M. Awad, A. Al-Dubai, R. Liu, C. Yuen, R. Raulefs, and E. Aboutanios, "Recent advances in indoor localization: A survey on theoretical approaches and applications," *IEEE Commun. Surveys Tuts.*, vol. 19, no. 2, pp. 1327–1346, 2nd Quart., 2017.
[7] *Apple Invents iBeacon Version 2 Using Ultra-Wide Band Radio Technology*. Accessed: Sep. 4, 2019. [Online]. Available: https://www.patentlyapple.com/patently-apple/2019/01/apple-invents-ibeacon-version-2-using-ultra-wide-band-radio-technology.html
[8] J. Karedal, S. Wyne, P. Almers, F. Tufvesson, and A. Molisch, "A measurement-based statistical model for industrial ultra-wideband channels," *IEEE Trans. Wireless Commun.*, vol. 6, no. 8, pp. 3028–3037, Aug. 2007.
[9] A. F. Molisch, "Ultra-wide-band propagation channels," *Proc. IEEE*, vol. 97, no. 2, pp. 353–371, Feb. 2009.
[10] C. Briso, C. Calvo, and Y. Xu, "UWB propagation measurements and modelling in large indoor environments," *IEEE Access*, vol. 7, pp. 41913–41920, 2019.
[11] H.-S. Lee, "A photon modeling method for the characterization of indoor optical wireless communication," *Prog. Electromagn. Res.*, vol. 92, pp. 121–136, Jan. 2009.
[12] M. Franceschetti, J. Bruck, and L. J. Schulman, "A random walk model of wave propagation," *IEEE Trans. Antennas Propag.*, vol. 52, no. 5, pp. 1304–1317, May 2004.
[13] A. G. Dimitriou and G. D. Sergiadis, "Architectural features and urban propagation," *IEEE Trans. Antennas Propag.*, vol. 54, no. 3, pp. 774–784, Mar. 2006.

[14] M. C. Lawton and J. P. McGeehan, "The application of a deterministic ray launching algorithm for the prediction of radio channel characteristics in small-cell environments," *IEEE Trans. Veh. Technol.*, vol. 43, no. 4, pp. 955–969, Nov. 1994.
[15] A. S. Glassner, *An Introduction to Ray Tracing*. New York, NY, USA: Academic, 1989.
[16] A. F. Molisch, J. R. Foerster, and M. Pendergrass, "Channel models for ultrawideband personal area networks," *IEEE Wireless Commun.*, vol. 10, no. 6, pp. 14–21, Dec. 2003.
[17] Z. Irahhauten, H. Nikookar, and G. J. M. Janssen, "An overview of ultra wide band indoor channel measurements and modeling," *IEEE Microw. Wireless Compon. Lett.*, vol. 14, no. 8, pp. 386–388, Aug. 2004.
[18] W. Ciccognani, A. Durantini, and D. Cassioli, "Time domain propagation measurements of the UWB indoor channel using PN-sequence in the FCC-compliant band 3.6-6 GHz," *IEEE Trans. Antennas Propag.*, vol. 53, no. 4, pp. 1542–1549, Apr. 2005.
[19] F.-G. Luan, P. Wang, and C. Chen, "Research on the frequency-dependent channel model of UWB in underground tunnel," in *Proc. 33rd Chin. Control Conf.*, Jul. 2014, pp. 7333–7337.
[20] D. B. Smith, D. Miniutti, T. A. Lamahewa, and L. W. Hanlen, "Propagation models for body-area networks: A survey and new outlook," *IEEE Antennas Propag. Mag.*, vol. 55, no. 5, pp. 97–117, Oct. 2013.
[21] A. Sani, A. Alomainy, G. Palikaras, Y. Nechayev, Y. Hao, C. Parini, and P. S. Hall, "Experimental characterization of UWB on-body radio channel in indoor environment considering different antennas," *IEEE Trans. Antennas Propag.*, vol. 58, no. 1, pp. 238–241, Jan. 2010.
[22] C. G. Spiliotopoulos and A. G. Kanatas, "Path-loss and time-dispersion parameters of UWB signals in a military airplane," *IEEE Antennas Wireless Propag. Lett.*, vol. 8, pp. 790–793, 2009.
[23] K. Haneda, J.-I. Takada, and T. Kobayashi, "Cluster properties investigated from a series of ultrawideband double directional propagation measurements in home environments," *IEEE Trans. Antennas Propag.*, vol. 54, no. 12, pp. 3778–3788, Dec. 2006.
[24] F. J. B. Barros, E. Costa, G. L. Siqueira, and J. R. Bergmann, "A site-specific beam tracing model of the UWB indoor radio propagation channel," *IEEE Trans. Antennas Propag.*, vol. 63, no. 8, pp. 3681–3694, Aug. 2015.
[25] T. Zasowski, G. Meyer, F. Althaus, and A. Wittneben, "UWB signal propagation at the human head," *IEEE Trans. Microw. Theory Techn.*, vol. 54, no. 4, pp. 1836–1845, Jun. 2006.
[26] A. Fathy, F. Newagy, and W. R. Anis, "Performance evaluation of UWB massive MIMO channels with favorable propagation features," *IEEE Access*, vol. 7, pp. 147010–147020, 2019.
[27] A. Khaleghi, I. Balansingham, and R. Chávez-Santiago, "Computational study of ultra-wideband wave propagation into the human chest," *IET Microw., Antennas Propag.*, vol. 5, no. 5, pp. 559–567, Apr. 2009.
[28] K. M. S. Thotahewa, J. Redoutè, and M. R. Yuce, "Propagation, power absorption, and temperature analysis of UWB wireless capsule endoscopy devices operating in the human body," *IEEE Trans. Microw. Theory Techn.*, vol. 63, no. 11, pp. 3823–3833, Nov. 2015.
[29] Q. Wang, T. Tayamachi, I. Kimura, and J. Wang, "An on-body channel model for UWB body area communications for various postures," *IEEE Trans. Antennas Propag.*, vol. 57, no. 4, pp. 991–998, Apr. 2009.
[30] T. Otim, A. Bahillo, L. E. Díez, P. Lopez-Iturri, and F. Falcone, "Impact of body wearable sensor positions on UWB ranging," *IEEE Sensors J.*, vol. 19, no. 23, pp. 11449–11457, Dec. 2019.
[31] T. Otim, A. Bahillo, L. E. Díez, P. Lopez-Iturri, and F. Falcone, "FDTD and empirical exploration of human body and UWB radiation interaction on TOF ranging," *IEEE Antennas Wireless Propag. Lett.*, vol. 18, no. 6, pp. 1119–1123, Jun. 2019.
[32] T. Otim, L. E. Díez, A. Bahillo, P. Lopez-Iturri, and F. Falcone, "Effects of the body wearable sensor position on the UWB localization accuracy," *Electronics*, vol. 8, no. 11, p. 1351, Nov. 2019.
[33] Q. Tian, K. I.-K. Wang, and Z. Salcic, "Human body shadowing effect on UWB-based ranging system for pedestrian tracking," *IEEE Trans. Instrum. Meas.*, vol. 68, no. 10, pp. 4028–4037, Oct. 2018.
[34] T. Otim, L. E. Díez, A. Bahillo, P. Lopez-Iturri, and F. Falcone, "A comparison of human body wearable sensor positions for UWB-based indoor localization," in *Proc. 10th Int. Conf. Indoor Positioning Indoor Navigat.*, Pisa, Italy, 2019, pp. 165–171. [Online]. Available: http://ceur-ws.org/Vol-2498/short22.pdf
[35] P. Leelatien, K. Ito, K. Saito, M. Sharma, and A. Alomainy, "Channel characteristics and wireless telemetry performance of transplanted organ monitoring system using ultrawideband communication," *IEEE J. Electromagn., RF Microw. Med. Biol.*, vol. 2, no. 2, pp. 94–101, Jun. 2018.
[36] P. Meissner, M. Gan, F. Mani, E. Leitinger, M. Frohle, C. Oestges, T. Zemen, and K. Witrisal, "On the use of ray tracing for performance prediction of UWB indoor localization systems," in *Proc. IEEE Int. Conf. Commun. Workshops (ICC)*, Budapest, Hungary, Jun. 2013, pp. 68–73.
[37] F. S. de Adana, O. Gutiérrez, M. A. Navarro, and A. S. Mohan, "Efficient time-domain ray-tracing technique for the analysis of ultra-wideband indoor environments including lossy materials and multiple effects," *Int. J. Antennas Propag.*, vol. 2009, pp. 1–8, Feb. 2009.
[38] M. Gan, P. Meissner, F. Mani, E. Leitinger, M. Frohle, C. Oestges, K. Witrisal, and T. Zemen, "Low-complexity sub-band divided ray tracing for UWB indoor channels," in *Proc. IEEE Wireless Commun. Netw. Conf. (WCNC)*, Istanbul, Turkey, Apr. 2014, pp. 305–310.
[39] C. Sturm, W. Sorgel, T. Kayser, and W. Wiesbeck, "Deterministic UWB wave propagation modeling for localization applications based on 3D ray tracing," in *IEEE MTT-S Int. Microw. Symp. Dig.*, Jun. 2006, pp. 2003–2006.
[40] G. Tiberi, S. Bertini, W. Q. Malik, A. Monorchio, D. J. Edwards, and G. Manara, "Analysis of realistic ultrawideband indoor communication channels by using an efficient ray-tracing based method," *IEEE Trans. Antennas Propag.*, vol. 57, no. 3, pp. 777–785, Mar. 2009.
[41] J. Jemai, P. C. F. Eggers, G. F. Pedersen, and T. Kurner, "Calibration of a UWB sub-band channel model using simulated annealing," *IEEE Trans. Antennas Propag.*, vol. 57, no. 10, pp. 3439–3443, Oct. 2009.
[42] W. Seesai, M. Chamchoy, and S. Promwong, "A body-shadowing model for indoor UWB communication environments," in *Proc. 5th Int. Conf. Electr. Eng./Electron., Comput., Telecommun. Inf. Technol.*, Krabi, Thailand, May 2008, pp. 261–264.
[43] L. Azpilicueta, F. Falcone, and R. Janaswamy, "A hybrid ray launching-diffusion equation approach for propagation prediction in complex indoor environments," *IEEE Antennas Wireless Propag. Lett.*, vol. 16, pp. 214–217, 2017.
[44] M. Celaya-Echarri, L. Azpilicueta, P. Lopez-Iturri, E. Aguirre, S. De Miguel-Bilbao, V. Ramos, and F. Falcone, "Spatial characterization of personal RF-EMF exposure in public transportation buses," *IEEE Access*, vol. 7, pp. 33038–33054, 2019.
[45] P. L. Iturri, E. Aguirre, L. Azpilicueta, U. Gárate, and F. Falcone, "ZigBee radio channel analysis in a complex vehicular environment [wireless corner]," *IEEE Antennas Propag. Mag.*, vol. 56, no. 4, pp. 232–245, Aug. 2014.
[46] E. Rajo-Iglesias, E. Aguirre, P. López, L. Azpilicueta, J. Arpón, and F. Falcone, "Characterization and consideration of topological impact of wireless propagation in a commercial aircraft environment [wireless corner]," *IEEE Antennas Propag. Mag.*, vol. 55, no. 6, pp. 240–258, Dec. 2013.
[47] E. Aguirre, P. Lopez-Iturri, L. Azpilicueta, A. Redondo, J. J. Astrain, J. Villadangos, A. Bahillo, A. Perallos, and F. Falcone, "Design and implementation of context aware applications with wireless sensor network support in urban train transportation environments," *IEEE Sensors J.*, vol. 17, no. 1, pp. 169–178, Jan. 2017.
[48] R. G. Kouyoumjian, "Asymptotic high-frequency methods," *Proc. IEEE*, vol. 53, no. 8, pp. 864–876, Aug. 1965.
[49] J. Keller, "Diffraction of a convex cylinder," *IRE Trans. Antennas Propag.*, vol. 4, no. 3, pp. 312–321, Jul. 1956.
[50] R. G. Kouyoumjian and P. H. Pathak, "A uniform geometrical theory of diffraction for an edge in a perfectly conducting surface," *Proc. IEEE*, vol. 62, no. 11, pp. 1448–1461, Nov. 1974.
[51] L. Azpilicueta, M. Rawat, K. Rawat, F. Ghannouchi, and F. Falcone, "Convergence analysis in deterministic 3D ray launching radio channel estimation in complex environments," *Appl. Comput. Electromagn. Soc. J.*, vol. 29, no. 4, p. 17, 2014.
[52] L. Azpilicueta, M. Rawat, K. Rawat, F. M. Ghannouchi, and F. Falcone, "A ray launching-neural network approach for radio wave propagation analysis in complex indoor environments," *IEEE Trans. Antennas Propag.*, vol. 62, no. 5, pp. 2777–2786, May 2014.
[53] F. Casino, L. Azpilicueta, P. Lopez-Iturri, E. Aguirre, F. Falcone, and A. Solanas, "Optimized wireless channel characterization in large complex environments by hybrid ray launching-collaborative filtering approach," *IEEE Antennas Wireless Propag. Lett.*, vol. 16, pp. 780–783, 2017.
[54] *Decawave MDEK1001 Kit User Manual*. Accessed: Jan. 12, 2019. [Online]. Available: https://www.decawave.com/sites/default/files/mdek1001_system_user_manual.pdf
[55] *Effects of Building Materials and Structures on Radiowave Propagation Above About 100 MHz*. Accessed: Apr. 12, 2020. [Online]. Available: https://www.itu.int/rec/R-REC-P.2040-1-201507-I/en

[56] A. F. Molisch, K. Balakrishnan, C.-C. Chong, S. Emami, A. Fort, J. Karedal, J. Kunisch, H. Schantz, U. Schuster, and K. Siwiak, *IEEE 802.15.4a Channel Model-Final Report*, IEEE Standard P802, 2004, vol. 15, no. 4, p. 0662.
[57] T. S. Rappaport, *Wireless Communications: Principles and Practice*, 2nd ed. Englewood Cliffs, NJ, USA: Prentice-Hall, 2001.
[58] E. Liebscher, "Approximation of distributions by using the anderson darling statistic," *Commun. Statist.-Theory Methods*, vol. 45, no. 22, pp. 6732–6745, Nov. 2016.
[59] R. Roess, E. Prassas, and W. McShane, *Traffic Engineering*, 2nd ed. Upper Saddle River, NJ, USA: Prentice-Hall, 2010.
[60] A. R. J. Ruiz and F. S. Granja, "Comparing ubisense, BeSpoon, and DecaWave UWB location systems: Indoor performance analysis," *IEEE Trans. Instrum. Meas.*, vol. 66, no. 8, pp. 2106–2117, Aug. 2017.

TIMOTHY OTIM received the B.Sc. degree in telecommunication engineering from Makerere University, Uganda, in 2012, and the M.Sc. degree in communication systems from Lund University, Sweden, in 2016, through a Full Scholarship from the Swedish Institute. He is currently pursuing the Ph.D. degree with the Mobility Research Group, DeustoTech-Fundación, University of Deusto, through the Research Training Grants Program. His main research interests include positioning and navigation systems, antenna technology, channel modeling, signal processing, and information theory.

PEIO LOPEZ-ITURRI (Member, IEEE) received the degree in telecommunications engineering, and the master's and Ph.D. degrees in communication engineering from the Public University of Navarre (UPNA), Pamplona, Navarre, in 2011, 2012, and 2017, respectively. He has worked in ten different public and private funded research projects. Since 2019, he has been working as a Researcher of Tafco Metawireless. He is also affiliated with the Institute for Smart Cities (ISC), UPNA. He has more than 120 contributions in indexed international journals, book chapters, and conferences. His research interests include radio propagation, wireless sensor networks, electromagnetic dosimetry, the modeling of radio interference sources, mobile radio systems, wireless power transfer, the IoT networks and devices, 5G communication systems, and EMI/EMC. He received the 2018 Best Spanish Ph.D. Thesis in Smart Cities from CAEPIA 2018 (third prize), sponsored by the Spanish Network on Research for Smart Cities CI-RTI and Sensors (ISSN 1424-8220). He was a recipient of the 2014 ECSA Best Paper Award and the 2015 IISA Best Paper Award.

LEYRE AZPILICUETA (Senior Member, IEEE) received the degree in telecommunications engineering, the master's degree in communications, and the Ph.D. degree in telecommunication technologies from the Public University of Navarre (UPNA), Spain, in 2009, 2011, and 2015, respectively. In 2010, she worked as a Radio Engineer with the Research and Development Department, RFID Osés. She is currently working as an Associate Professor and a Researcher with the Tecnologico de Monterrey, Monterrey, Mexico. She has over 150 contributions in relevant journals and conference publications. She was a recipient of the IEEE Antennas and Propagation Society Doctoral Research Award, in 2014, the Young Professors and Researchers Santander Universities Mobility Award, in 2014, the ECSA Best Paper Award, in 2014, the IISA Best Paper Award, in 2015, the Best Ph.D. awarded by the Colegio Oficial de Ingenieros de Telecomunicación, in 2016, and the N2Women: Rising Stars in Computer Networking and Communications Award, in 2018.

ALFONSO BAHILLO received the degree in telecommunications engineering and the Ph.D. degree from the University of Valladolid, Spain, in 2006 and 2010, respectively, and the PMP Certification from the PMI, in 2014.

From 2006 to 2010, he joined CEDETEL, as a Research Engineer. From 2006 to 2011, he was an Assistant Professor with the University of Valladolid. From 2010 to 2012, he was with LUCE Innovative Technologies, as a Product Owner. From 2013 to 2017, he held a postdoctoral position and was the Project Manager of DeustoTech-Fundación, Bilbao, where he trains Ph.D. degree students and collaborates with several national and international research projects. He has worked (leading some of them) in more than 25 regional, national, and international research projects and contracts. He is currently the Director of DeustoTech-Fundación, University of Deusto, Bilbao. He has coauthored 20 research manuscripts published in international journals and more than 40 communications in international conferences, and holds three national patents. His research interests include local and global positioning techniques, ambient assisted living, intelligent transport systems, wireless networking, and smart cities.

LUIS ENRIQUE DÍEZ received the degree in telecommunications engineering from the University of Deusto, in 2005, the M.Sc. degree in communication technologies and systems from the Polytechnic University of Madrid, in 2012, and the Ph.D. degree from the University of Deusto, in 2019.

From 2005 to 2011, he was a Senior IT Consultant with Everis. From 2013 to 2014, he was a Research Support Technician with the SOFTLAB Research Group, University Carlos III of Madrid (UC3M). Since 2014, he has been with the Mobility Research Group, DeustoTech-Fundación, University of Deusto, Bilbao, Spain. His research interests include pedestrian navigation systems, data fusion techniques, and context-aware applications.

FRANCISCO FALCONE (Senior Member, IEEE) received the degree in telecommunication engineering and the Ph.D. degree in communication engineering from the Public University of Navarre (UPNA), Spain, in 1999 and 2005, respectively. From 1999 to 2000, he was a Microwave Commissioning Engineer with Siemens–Italtel, deploying microwave access systems. From 2000 to 2008, he was a Radio Access Engineer with Telefónica Móviles, performing radio network planning and optimization tasks in mobile network deployment. In 2009, he was a Co-Founding Member and the Director of Tafco Metawireless, a spin-off company from UPNA, until 2009. He was an Assistant Lecturer with the Department of Electrical and Electronics Engineering, UPNA, from 2003 to 2009. In 2009, he became an Associate Professor with the Department of EE, where he was also the Department Head, from 2012 to 2018. From January 2018 to May 2018, he was a Visiting Professor with the Kuwait College of Science and Technology, Kuwait. He is also affiliated with the Institute for Smart Cities (ISC), UPNA, which hosts around 140 researchers, and currently acting as the Head of the ICT Section. He has more than 500 contributions in indexed international journals, book chapters, and conferences. His research interest includes computational electromagnetics applied to the analysis of complex electromagnetic scenarios, with a focus on the analysis, design, and implementation of heterogeneous wireless networks to enable context-aware environments. He was a recipient of the CST 2003 and CST 2005 Best Paper Award, the Ph.D. Award from the Colegio Oficial de Ingenieros de Telecomunicación (COIT), in 2006, the Doctoral Award from UPNA, in 2010, the First Juan Gomez Peñalver Research Award from the Royal Academy of Engineering of Spain, in 2010, the XII Talgo Innovation Award, in 2012, the IEEE Best Paper Award, in 2014, the ECSA-3 Best Paper Award, in 2016, and the ECSA-4 Best Paper Award, in 2017.